04

Fast shadow visualization of a pulsed discharge in a short gas gap

© S.G. Davydov, A.N. Dolgov, A.A. Kozlov, V.O. Revazov, R.Kh. Yakubov

Dukhov All-Russia Research Institute of Automatics, Moscow, Russia
e-mail: vniia4@vniia.ru

Received April 14, 2022
Revised July 3, 2022
Accepted July 3, 2022

A study of the switching process of a short (1 mm) gas gap initiated by a spark discharge along the dielectric surface was carried out by the method of shadowgraphy with nanosecond time resolution. The presence of a shock wave propagating from the cathode spot and signs of intermediate accumulation of the invested energy in the form of excitation energy of gas molecules or turbulent gas flow were detected.

Keywords: shadowgraphy, gas discharge, shock waves, switch.

DOI: 10.21883/TP.2022.10.54358.106-22

Introduction

The study of shock waves (SW) is of interest not only for fundamental science, but also from the point of view of practical application. Recently, a comparatively new area of plasma physics, i.e. plasma aerodynamics, has been intensively developed. The problems of plasma aerodynamics are related to the interaction of plasma formations with high-speed air flows and various gas mixtures. An electric discharge in gas is considered as an effective way of supplying energy to gas flow as a result of the Joule dissipation of the electric current energy of the discharge [1,2]. From a practical point of view, this can be used, for example, to rearrange shock-wave configurations in front of an aircraft by controlling the flow field, or it can be used as an effective way to ignite air-fuel mixtures in engines. Shock-wave phenomena occur with a large energy input in a small volume in a short period of time, for example, during spark discharges in air. Note that the gas flow caused by spark discharge differs from an instantaneous explosion, since the time of SW movement is comparable with the time of energy release. The physical pattern of the phenomena arising during the shock waves propagation in a thermally non-equilibrium weakly ionized plasma has not been sufficiently studied so far, due to the complexity of this pattern.

This paper presents the results of studying the switching process of a short air gap, initiated by an auxiliary spark discharge over the dielectric surface, using the shadow visualization method with nanosecond time resolution. Further in the text we will sometimes use the term shadowgraphy for short.

1. Scheme of experiment

In the studies carried out, a compact gas-filled discharge device was used. The discharge device was a three-electrode system, the main elements of which are the cathode that ignites the electrode, and the dielectric washer that separates the cathode from the igniting electrode, and a separate anode (Fig. 1).

An auxiliary initiating spark discharge goes over the surface of the dielectric (corundum-type ceramic) washer 0.4 mm thick in the surface area closest to the anode surface, between the earthed cathode and the igniting electrode when a high-voltage pulse of positive polarity and an amplitude of up to 3 kV is applied to the igniting electrode. The duration of the initiating discharge is less than $0.1\,\mu$s. Current amplitude — up to 10 A. The main arc discharge occurs between the cylindrical cathode and the conical anode, which is under a positive potential of 3.5 kV. The discharge in the cathode–anode gap 1 mm long was initiated in air at atmospheric pressure. The discharge was damped current oscillations with a period of $2\,\mu$s, the amplitude of which in the first half-cycle of the discharge reached 4.5 kA. The discharge goes into the short circuit mode within a time interval less than $0.2\,\mu$s after the start of the initiating discharge [3].

As a source of probing radiation we used a pulsed solid-state laser emitting a light pulse 2.5 ns wide at half maximum with a carrier wavelength $\lambda = 1.06\,\mu$m. A

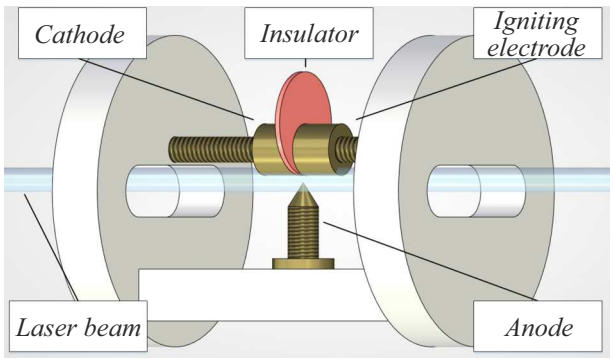

Figure 1. Scheme of the experiment on obtaining shadow images of discharge by means of transmission by beam of pulsed laser.

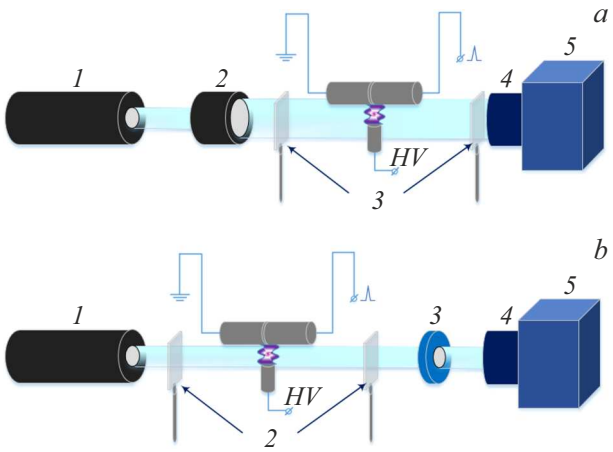

Figure 2. *a* — first version of the optical scheme of the experiment: *1* — probing laser, *2* — zoom lens, *3* — optical filters, *4* — zoom lens, *5* — video camera; *b* — second version of the optical scheme of the experiment: *1* — probing laser, *2* — optical filters, *3* — diaphragm with aperture 3 mm, *4* — zoom lens, *5* — video camera.

delayed pulse generator was used to synchronize the laser triggering and the generation of an initiating high-voltage pulse. The diameter of the practically parallel radiation beam at the laser output was about 3 mm. The probing of the object under study was carried out in two options (Fig. 2). In the first option, with the help of an auxiliary lens the diameter of the laser radiation beam was preliminarily increased by 2 times in order to expand the probing area and simplify alignment, and then the already broadened radiation beam transmitted through the discharge device as shown in Fig. 1. Next, the probing radiation enters another lens, which produced additional beam broadening, which made it possible to obtain zoomed image of the object. Then the beam entered the input window of the OPHIR Spiricon BGS−USB−SP928−OSI high-speed video camera, which recorded the shadow image of the object under study in the wavelength range 190−1100 nm with a single frame exposure time of 60 μs. In the second option, the laser radiation beam without preliminary broadening was used to probe the object under study, but the radiation that transmitted through the discharge region was collimated, which reduced the contribution to the formed discharge image of part of the laser radiation that, under the influence of the refraction phenomenon, deviated from the initial direction of propagation.

In the first case, we obtained a scheme for shadow probing by a parallel beam with an increased spatial resolution. In the second case, the scheme for probing the object under study was implemented, which was more responsive to areas with a high density gradient of the material. In each discharge, a single shadow image of the cathode−anode gap was recorded with a certain time reference relative to the moment of switching the circuit of the initiating spark discharge over the dielectric surface.

Using the software of the system for digital processing and forming image captured by video camera, allowed backlight „subtracting“The selection of appropriate absorbing optical filters placed in the path of laser radiation propagation made it possible, on the one hand, to cut out a narrow wavelength range near the carrier wave of laser radiation $\lambda = 1.06\,\mu$m and completely eliminate the plasma glow. On the other hand, the selection of filters ensured such a value of the intensity of laser radiation reaching the video camera, at which there was no supersaturation of the video camera pixels, but the resulting image, in turn, was quite bright. Images below in the text are shown in color for the following reasons. The laser-illuminator used by us, i.e. the source of probing radiation has a rather heterogeneous radiation field in the cross-section. Under these conditions the use of color palette makes it easier to separate in the resulting image the heterogeneities, due to the quality of the probing radiation source, from optical heterogeneities in the object under study. The vertical color bar in the right side of the corresponding Figures demonstrates the relative intensity (or energy fluence) of the transmitted probing radiation — when moving from bottom to top, this parameter increases.

During the experiments the following oscillograms were recorded: the pulsed voltage applied to the ignition electrode; the current strength in the cathode−anode gap, the signal from the photosensor, which fixes the pulse of the probing laser radiation (Fig. 3). All this made it possible to temporally link the recorded images to the phase of the discharges development, both initiating and main.

2. Results of using two optical schemes

An analysis of the images obtained in a series of experiments using the scheme of shadow probing by parallel beam makes it possible to register the features of the spatial structure of the optical medium during discharge in the region of the cathode−anode interelectrode gap. The obtained images (Fig. 4) in the region of the main discharge between the cathode and the anode reflect the process of SW propagation in the gas, and initially it is close to cylindrical coaxial to the anode, and then transforms into a spherical wave as it propagates. Two density jumps (DJ) are observed, i.e. two areas of discontinuity. The first of them (front) corresponds to the SW front, the second (rear) — possibly represents the contact boundary between the SW front and the current flow channel. If this assumption is correct, then from the very beginning and up to the time 0.8 μs after the start of the discharge, the SW has a velocity greater than the current channel expansion speed. And at the time about 1.2 μs after the start, the SW is separated from the current channel, and the image of the second DJ is not visually fixed further.

The SW formation is due to the current channel expansion into the environment at supersonic speed. The geometric shape of the anode used, due to the corresponding spatial

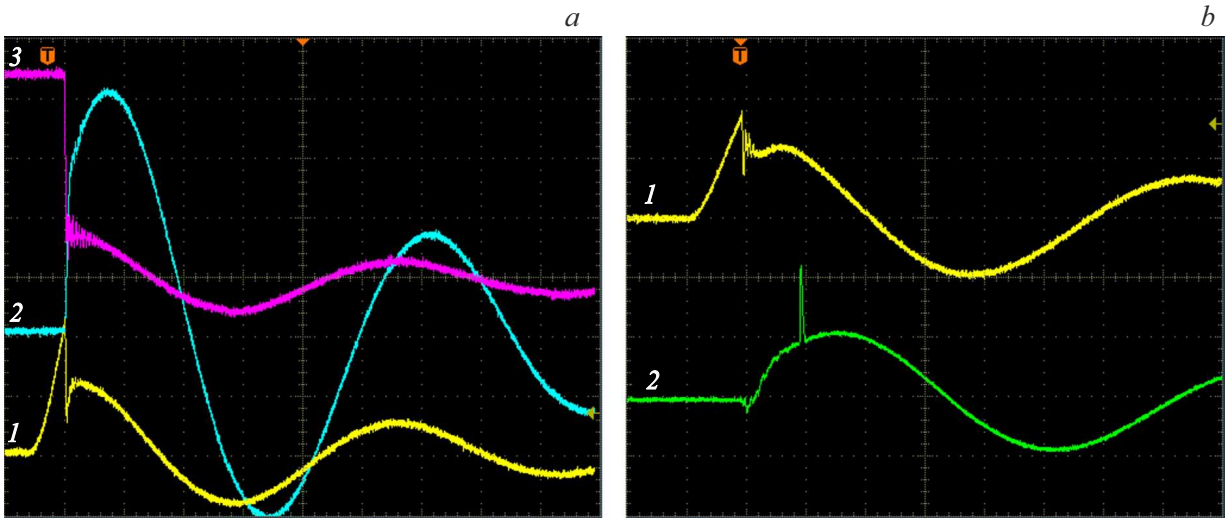

Figure 3. Oscillograms of the signals recorded in the experiment: *a* — beam № 1 — voltage in the gap cathode–ignition electrode, beam № 2 — current in the gap cathode–anode, beam № 3 — voltage in the gap cathode–anode. Sensitivity: beam № 1 — 1 kV/div, beam № 2 — 1 kA/div, beam № 3 — 1 kV/div; *b* — beam № 1 — voltage in the gap cathode–igniting electrode, beam № 2 — signal from photosensor that detects a pulse of probing laser radiation. Sensitivity: beam № 1 —1 kV/div, beam № 2 — 2kV/div. Sweep — 400 ns. The stage rumble of current flowing in the discharge circuit in the cathode–anode gap is superimposed on signal from the photodetector.

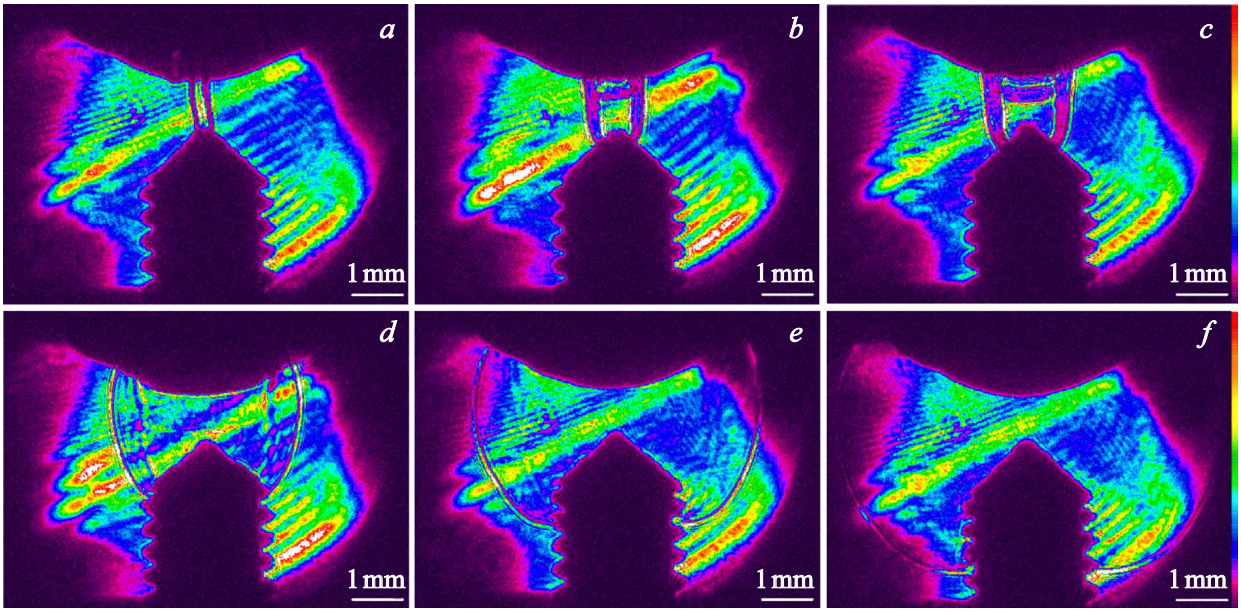

Figure 4. Images of the cathode–anode spatial region, recorded after 0.4 (*a*), 0.7 (*b*), 0.8 (*c*), 1.2 (*d*), 2.0 (*e*), 3.2 μs (*f*) from the start of current flow in the main discharge. The images were obtained using the optical scheme of shadow probing with a parallel beam.

structure of the electric field, ensures the predominant development of the discharge along the symmetry axis of the anode (or near it). Besides, the use of broadened beam of probing radiation made it possible to spatially link the observed objects in a rather wide time interval.

It can be seen that in the DJ region in the SW front the substance is optically denser than before the wave front, but it remains partially optically transparent. At the same time, it can be noted that immediately behind the first DJ, where the so-called relaxation zone should be, we observe a certain transition layer, a substance that turns out to be optically small and transparent to the probing radiation. Moreover, the thickness of this layer between the first and second DJs gradually increases, at least at the stage of a cylindrical wave. One can pay attention to the fact that this transition layer is clearly visible in the images of a cylindrical shock wave, and as it passes to the stage of spherical wave, it becomes clear and becomes invisible.

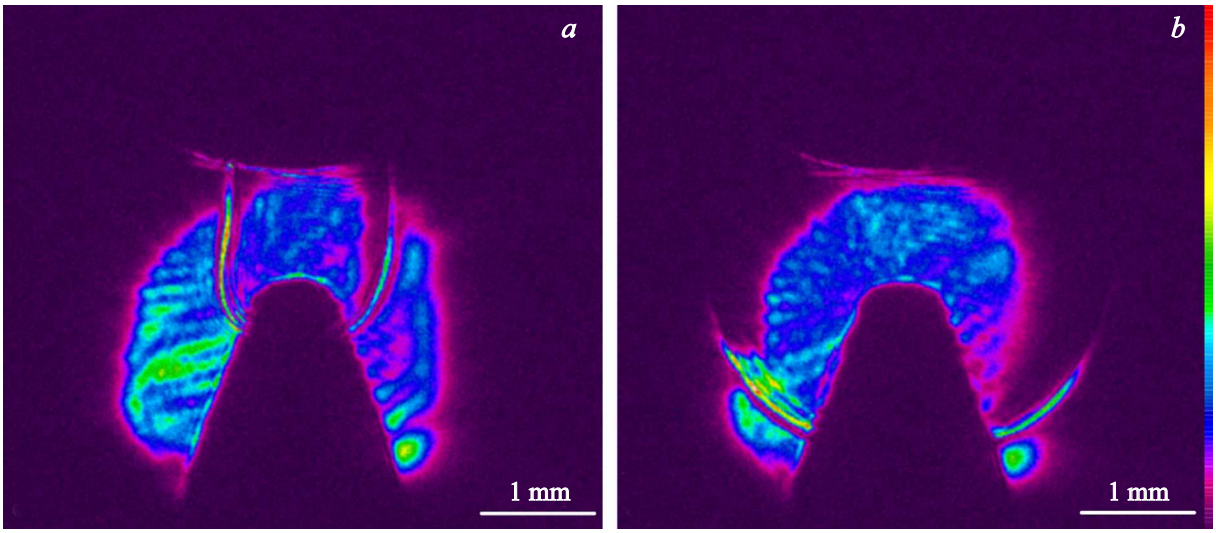

Figure 5. Images of the cathode–anode spatial region recorded after 0.9 (a) and 1.2 μs (b) of start of current flow in the main discharge. The images were obtained using the optical scheme with collimation of the probing laser radiation transmitted through the object under study.

The DJ has the largest gradient in the shock wave front due to its small thickness — theoretically on the order of the free path length of particles in the gas. The density of matter behind the DJ also has a gradient [4].

It is interesting to note that in this series of experiments, in addition to images of the shock wave created by the current channel of the main discharge, we were able to observe an image of another object located inside the region already subjected to the shock compression process (Fig. 4, *a, b*). This is a narrow area of space with a slightly curved shape, elongated in the direction perpendicular to the surface of the cylindrical shock wave, characterized by a reduced intensity of the probing radiation transmitted through it and very similar in thickness and intensity of the transmitted radiation to the images of the spherical shock wave of the spark channel. The direction of the bend suggests that this is shock wave or a cathode flame propagating from small ($\leq 100\,\mu$m) region on the cathode surface. Separately note that when using this optical system in the case of the main discharge initiation in vacuum, we did not observe not only shock waves, which is quite natural, but also any signs of the density increasing of the matter in the interelectrode gap, for example, in the form of a cathode or anode flame ejection. The conclusion suggests itself that we are observing rather shock wave created as a result of the matter ejection from the cathode spot of a spark and then arc discharge or as a result of the broadening of the spark discharge channel over the surface of the dielectric, but not the front of the cathode flame. The cathode spot is localized near the place where the breakdown occurred over the surface of the dielectric separating the cathode and the igniting electrode, this is shown by the observed nature of the erosion of the cathode surface.

In a series of experiments using the scheme without preliminary broadening of the probing beam and collimating the probing radiation that passed through the discharge region, the shape of the anode was somewhat changed. The opening angle of the cone was reduced and the radius of curvature of its top was increased in order to provide the possibility of observing both the cylindrical and spherical stages of shock wave development under conditions of reduced diameter of the probing radiation beam (Fig. 5).

The change in the optical scheme of the experiment led to noticeable changes in the nature of the recorded images. First, in the SW front the narrow regions of first clearing and then — shadowing followed one after another, which was caused by the DJ presence and the corresponding refraction index gradient. Now, another narrow but clearly observable shadowing zone appeared in front of the indicated region of clearing , which is probably located in front of the SW front. In this case the feature of the optical probing scheme suggests that in this newly discovered region of space, the matter is in a state that leads to strong scattering of probing radiation by refraction index gradients. For example, this can be a state of turbulence (vortex), i.e. multiple chaotic density jumps are formed in this region of space. Secondly, in general, the image of the region behind the SW front turns out to be shadowed compared to the space in front of the SW front, which was not observed in the first probing option. Again, this circumstance may be due to the turbulent state of matter. Thirdly, the most obvious difference is the appearance of region immediately behind the SW front, both at the stage of cylindrical and spherical wave, which is completely impervious to probing radiation. Moreover, the width of this region is the largest at the cathode surface, and gradually decreases towards the anode, and only increases with time. Fourth, it should be noted

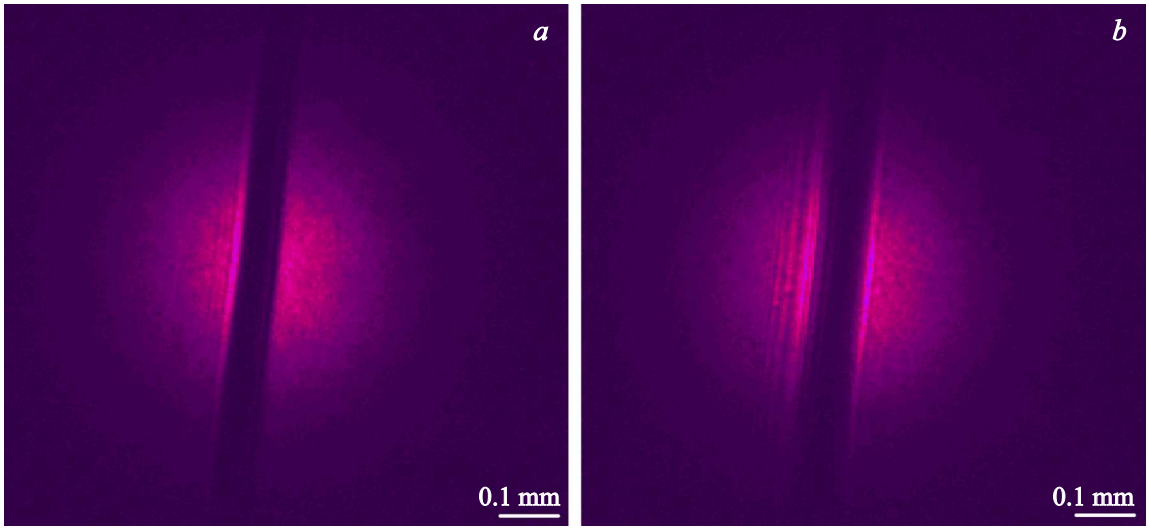

Figure 6. Wire shadow images: *a* — „good“ focusing, no diffraction pattern observed; a glare is visible on the wire on the left; *b* — „poor“ focusing, diffraction pattern observed.

that the object previously regularly present (when using the scheme of shadow probing with parallel beam) in the images, propagating along the axis of the main discharge and treated above according to assumption as a SW from the region of cathode spot formation, was not observed in this setting of the experiment.

Thus, comparing the nature of the images of the cathode–anode interelectrode gap recorded using two optical schemes during the arc discharge development, the following circumstances can be noted. After the passage of SW due to the development of the arc discharge channel, the gaseous medium is in a special optical state almost during the entire observation time and has an increased ability to absorb and to scatter the probing radiation. To the greatest extent these properties are found in a certain transition layer (or, more precisely, two layers of probably different nature) located immediately behind the DJ in the shock wave front and having a thickness of 0.08–0.6 mm during shadow probing and 0.2–1.2 mm when probing with the collimation of the transmitted radiation. In both cases, the layer thickness increasing with time is observed. In the first case, the transition layer is semitransparent to the probing radiation and its thickness is approximately the same along the SW front and has a well-defined rear boundary at the cylindrical wave stage. We identified it as zone of relaxation. It can be assumed that the relaxation zone located between the two recorded DJs, on the one hand, plays the role of a contact boundary between the shock wave front and the current flow channel, and on the other hand, it plays the role of a piston that causes the shock wave appearance. In the second case, the transition layer is completely opaque to the probing radiation, and the layer thickness is greatest at the cathode and gradually decreases when approaching the anode until the layer disappears completely. In the first case, the transition layer is observed only at the stage of a cylindrical wave and disappears when the wave transforms into a spherical one. Secondly, the layer presence is fixed both at the cylindrical wave stage and at the spherical wave stage.

When using the optical scheme of shadow probing the object was found that has increased ability to absorb and to scatter probing radiation, and propagates in the area exposed to the shock wave in the direction from the cathode to the anode. This object was regularly observed at the cylindrical wave stage. At the stage of the cylindrical wave transformation into the spherical wave (0.8 μs after the start of the main discharge), and then the object ceases to be registered. When using the optical probing scheme with the collimation of the transmitted radiation, such object was not observed.

Coherent laser radiation will experience diffraction at the shock wave front if its thickness is comparable to the radiation wavelength. Theoretically, this is how it should be. Technically, we are unable to observe the gas-dynamic discontinuity of such a magnitude, for example, due to the image blurring as a result of refraction [5]. Probably, there are also physical reasons for the real blurring of the SW front, for example, the penetration behind the SW front of electrons and radiation, which ionize the neutral gas [4].

The analysis of the publications provides additional food for thought. High-quality shadow images of dense plasma of discharges in vacuum do not reveal diffraction traces [6–8]. High-quality images of SW in a dense gas, arising under the action of bodies moving at supersonic speed, do not reveal any diffraction traces [5]. The authors [9] obtained shadow images of the cathode plasma at the initial stage of the discharge in gas, at that a 30 μm wire acted as the cathode, and also we did not observe anything similar to the interference fringes. The paper [10] presents shadow images of laser plasma of the products of ablation of a solid

target in the atmosphere, on which there are no diffraction traces. Some reports feature shadow images bearing traces of striped structures resembling the diffraction pattern. For example, in [11] images of the edge of a high-pressure gas region heated by laser beam show periodic structures similar to interference fringes. The paper [12] shows images of laser plasma from products of ablation in air, and fringes similar to interference fringes are seen in some places on the edge of the plasma flame. Perhaps the most interesting result in this case was obtained by the authors of the paper [13]. When obtaining shadowgrams of the laser plasma flame in atmospheric air, the following circumstance was discovered. The observed fringes width (DJ, etc.) depends on the focus point of the video camera. When focusing at the center of SW, the image of its front has a minimum thickness; besides, nothing similar to interference fringes is observed. When the focus point is changed (closer, farther), the thickness of the front image increases, and fringes similar to interference ones appear. In all the above examples, we are talking about the shadow visualization of various objects using the pulse of laser radiation in the optical range of nanosecond or less width. Let us make some conclusion from the above data. Probably, the presence or absence of the diffraction pattern in obtained by the shadow method images of macroobjects, similar to those described above, with significant optical density gradients, is determined primarily by the quality of focusing of the optical system that forms the image. Besides, it is entirely possible that the flow of electrons and radiation capable of ionizing neutral matter ahead of the SW front can lead to the formation of certain periodic structures in the plasma ahead of the SW front [14].

A control experiment was carried out. A wire with a diameter of $70\,\mu$m was placed at the place of the object under study, and its shadow images were obtained using the laser illuminator (helium-neon laser with $\lambda = 0.622\,\mu$m), shown in Fig. 6.

Under the conditions of „good“ focusing of the video camera on the wire, we observed a distinct image of the wire, and there is no diffraction pattern. Under „poor“ focusing conditions, the wire image is somewhat blurred, and a diffraction pattern is observed, the width of the fringes is independent of the degree of defocusing. The total width of the first (widest) diffraction fringe (which is proportional to $(\lambda)^{1/2}$) recalculated to the operating wavelength of the probing radiation will be $30\,\mu$m for the object, while the width of the registered area of the density jump in the SW front is $\sim 140\,\mu$m, and the minimum width of the elements of the registered spatial structure of the discharge, which is similar to the diffraction pattern, is $\sim 120\,\mu$m. This leads to the conclusion that the phenomenon of diffraction, even when the focusing of the optical system is not the most successful (which is inevitable for some observed evolutions of the geometry of the object under study from discharge to discharge, with its overall good repeatability), is not capable of masking the real features of the recorded images. The achieved spatial resolution can be taken equal to at least half of the wire diameter, i.e. $\sim 35\,\mu$m.

3. Analysis of results of spatial structure observation of shock waves

The results of one of the series of experiments are displayed as the observed displacement of the shock wave front (more precisely, the DJ) formed under the action of the main discharge in the direction transverse to the discharge gap axis $r_{dis}(t)$ versus the time elapsed from the moment the current of the main discharge begins to flow (Fig. 7).

The nature of the resulting diagram is similar to the nature of similar (or analogue to it) graphs given in the scientific literature by other authors [4,14–19]. Most authors give diagrams of the dependence $r_{dis}(t)$ for shock waves in dense gases, which also contain a linear section corresponding to a rather late phase of wave front propagation with a constant velocity $\sim 10^2-10^3$ m/s. It is considered to be reliably established that the section of the diagram under consideration corresponds to the situation of the SW front separation from the walls of the discharge channel. The authors [5,9] present diagrams with two almost linear segments corresponding to two different velocities. At the early stage — higher speed, at the late stage — it is lower than early stage speed by an order of magnitude.

There is, however, a significant difference from the results obtained by us. The initial portion of the dependence $r_{dis}(t)$ obtained in the specified papers does not have an knee point corresponding to the maximum velocity of wave propagation, as is observed in our case. The linear section of our diagram corresponds to the velocity equal to $8 \cdot 10^2$ m/s, but the maximum velocity in the initial (nonlinear in our diagram) section significantly exceeds this value and lies in

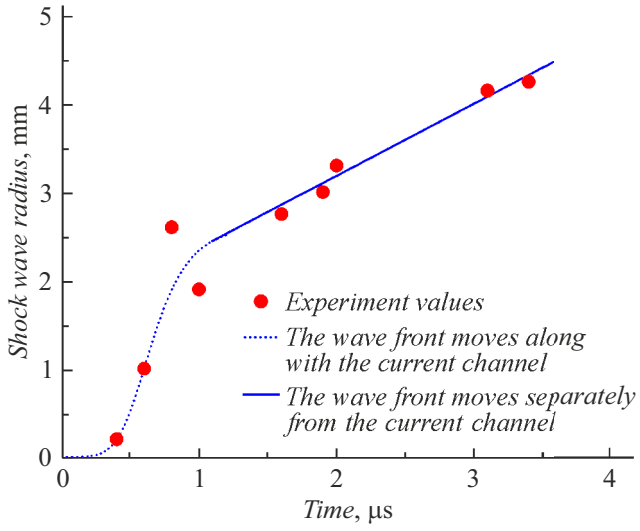

Figure 7. Displacement of SW, formed during the formation of the main discharge channel, in the direction perpendicular to the discharge axis, vs. time elapsed from the moment the current begins to flow in the discharge. The displacement is measured from the discharge axis. Measurement error is within experimental points.

the range $(4-5) \cdot 10^3$ m/s. At the same time, it must be recognized that if we allow the existence of the knee point in the nonlinear section of the diagram, then there must be a section of slow expansion that precedes the region where the velocity reaches its maximum. The velocity corresponding to this section (below 250 ns) on our diagram is $\sim (4-5) \cdot 10^2$ m/s. The authors of paper [20] observed during self-breakdown of a short gas gap in with similar geometry of the electrode system immediately after the start of the system formation of microchannels broadening at the same velocity, up to the moment of the channels merging in 20 ns after the start. Using the data of the authors of the paper [4], one can estimate the temperature and relative compaction of the medium behind the shock wave front. For the section where the maximum velocity of the wave front is reached — 6000 K and ~ 10. The given temperature value agrees with the known temperature values in the cathode spot, fixed by spectroscopy methods in the optical range [21].

As regards the object we discovered, which propagates along the axis of the main discharge in the direction from the cathode to the anode, we will first must to return to the question of its nature.

As an alternative to the already proposed hypothesis that this object is SW, the assumption can be made about the phenomenon that is observed in various plasma experiments such as, for example, glow discharge, laser plasma, self-compressed discharges (Z-pinches), exploding wires and liners. We are talking about the phenomenon of stratification of the plasma column (or plasma flame). Note at once that the phenomenon of stratification in each such experiment is given by reasons of a quite definite nature. When the laser plasma expands in the background gas, the density stratification is observed behind the SW front and arises due to the separation of the laser plasma and the SW [22,23] by the contact interface, which does not contradict our hypothesis. Moreover, at the intensity of laser radiation in the focusing spot $\sim 10^9$ W/cm^2, SW begins to form even in a solid target [24]. Note that in the centers of explosive emission of electrons forming the cathode spot, exactly this or even higher energy flux density is achieved [25]. If the target material has a complex elemental composition, then due to the Coulomb interaction of charged particles in the plasma the spatial separation of the plasma bunch by atomic masses is possible, but in a rarefied gas [26], which does not correspond to our conditions. In glow discharge the process leading to stratification (the appearance of ionization waves) is the ionization by electron impact of there again rarefied gas and the drift transfer of electrons [27–29]. In exploding liners, implemented by passing megaampere currents, a spatial plasma structure arises in the form of radially elongated bunches as a result of a magnetic flux breakthrough due to a violation of the local balance between the supply and ionization of the plasma-forming substance on the one hand, and its removal by Ampere forces from the plasma formation zone on the other hand [30]. Plasma stratification

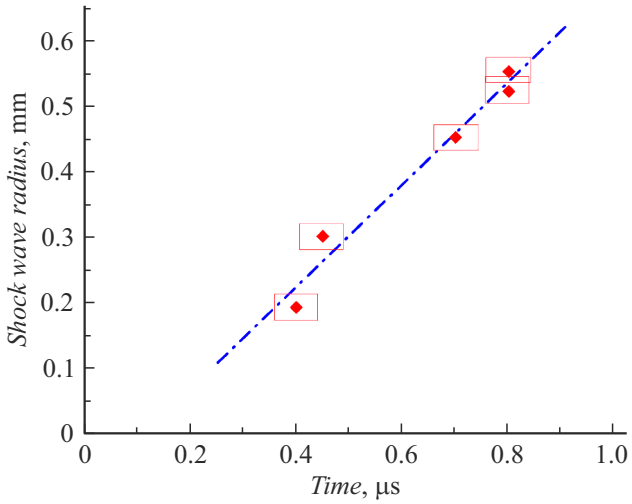

Figure 8. Movement of object propagating along the main discharge channel vs. time elapsed since the start of the discharge. The displacement is measured from the cathode surface.

transverse with respect to the discharge axis in Z-pinches is caused by an imbalance between the gas-kinetic pressure of the plasma and the magnetic field pressure of the discharge current ~ 10 kA or more, which leads to the development of magnetohydrodynamic instability and the formation of local waists and radial plasma ejections [6]. Thus, the validity of the hypothesis about the nature of the object propagating along the axis of the main discharge in the direction from the cathode to the anode is confirmed.

The dependence of the movement $r_{cp}(t)$ of the object we detected, propagating along the channel of the main discharge, on the time elapsed since the start of the discharge is shown in Fig. 8.

With a linear extrapolation of this dependence, the average value of the propagation velocity of the object under consideration will be $8 \cdot 10^2$ m/s. The obtained value is comparable with the thermal velocity of atomic particles $\sim 10^3$ m/s, which can be emitted from the cathode spot in accordance with the results of measurements of the substance temperature in the cathode spot $\sim 0.2-0.6$ eV, performed by methods of spectroscopy in the visible range [21]. An even higher speed (10^4 m/s and more) is exhibited by particles emitted with a plasma flow from the cathode spot region, the particles were detected in the course of measurements by the Langmuir electrostatic probe when initiating a discharge in vacuum [31].

From the fact of the slow propagation of the specified object along the main discharge channel, the following conclusion must be made. The assumption put forward by some authors that SW formation caused by the appearance of cathode spot, which, propagating in the main discharge channel, leads to additional heating and ionization of the substance in it, and is the reason for the channel transformation into a spark one, which has a high conductivity [19,32,33], is not confirmed. If we assume that the object

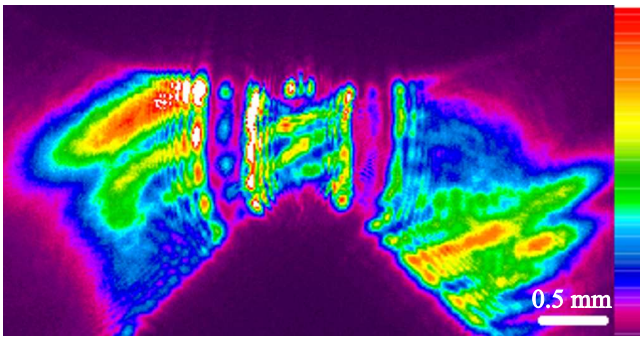

Figure 9. Image of the cathode–anode spatial region with a spherical object near the cathode. The image was obtained using the optical scheme of shadow probing with parallel beam.

under consideration is SW, then the overlapping time of the cathode–anode gap shall be $\sim 1.2\,\mu$s. However, based on the oscillograms, the discharge goes into the short circuit mode, i.e. in an arc one, already in $0.2\,\mu$s [3] after the start. Also note that in the course of our series of experiments, we failed to capture the image of SW propagating along the main current channel later than $0.8\,\mu$s after the start of the discharge.

Let us try, by analyzing the available data, to present the mechanism of this shock wave excitation. The power released in the area of the cathode spot can be estimated as the product of the current in the discharge and the cathode potential drop ~ 20 V. We estimate the power dissipated in the discharge as the product of the current strength and the potential difference between the cathode and the anode. By the time $0.4\,\mu$s after the start, when it is possible to register the object propagating along the axis of the main discharge, the energy released in the main discharge will be $\sim 4 \cdot 10^{-1}$ J, and the energy released in cathode spot area will be $\sim 3 \cdot 10^{-2}$ J. At the same time, the energy released in the initiating discharge over the dielectric surface is only $\sim 10^{-5}$ J [34]. Thus, the observed presumably SW propagating along the axis of the main discharge can hardly be the result of broadening of the spark discharge channel over the dielectric surface. Probably its source is the area of the cathode spot of the main discharge. But the cathode flame matter does not play the role of the piston. When using this optical scheme during the initiation of the discharge in vacuum, the presence of the matter of the cathode flame was not registered by shadow visualization methods. When initiating in a gaseous medium, there are again no observable signs of the cathode flame formation. The SW generators could be regular plasma bunches emitted from the centers of explosive electron emission [25].

Let us pay attention to the fact that the initially spherical object (Fig. 9), which is formed on the cathode surface and then propagates along the axis of the main discharge in the direction of the anode, turns into shock wave, which acquires almost flat shape.

This object does not go beyond the region limited by cylindrical SW caused by the main discharge in the cathode–anode gap. It would be appropriate to assume that this object transformation into shock wave close in shape to a flat one occurs precisely due to the interaction of two shock waves, i.e. the one formed under the action of the broadening main discharge channel, and the another formed in the region of the cathode spot. One of the effects, that occurs when shock waves are (obliquely) reflected from the obstacle surface, is the third wave generation, called a Mach wave, which propagates in parallel to the reflecting plane [35]. Another important effect associated with the occurrence of Mach waves is the propagation of spherical shock waves enclosed inside cylindrical channel. The authors [36] have shown that spherical shock front is transformed into a flat front during propagation inside the cylindrical channel due to reflection with the formation of Mach waves. Thus, it is possible that we observed the transformation of the spherical shock wave into the plane wave upon reflection from the front of the cylindrical SW and the generation of Mach waves.

It was noted that during the series executed it was not possible to fix images of SW propagating along the axis of the main discharge after $0.8\,\mu$s since the start of the discharge flowing in the cathode–anode gap. Let us try to explain this phenomenon. It is known that when a supersonic gas flow propagates into a more rarefied gas medium, a rarefaction wave [37] is formed. Note that before the SW front, i.e. of compression wave propagating along the axis of the main discharge, the rarefaction wave is actually observed (Fig. 10), and the compression region is observed near the anode surface, apparently as a result of the oncoming flow of matter. May be the collision of these three objects leads to SW relaxation, not reaching the anode surface. Another possible explanation is that the Mach wave ceases to occur when the cavity walls, in which it is formed, lose their cylindrical shape.

There is another interesting question, and it is as follows. What is the reason for the fact that such a sudden

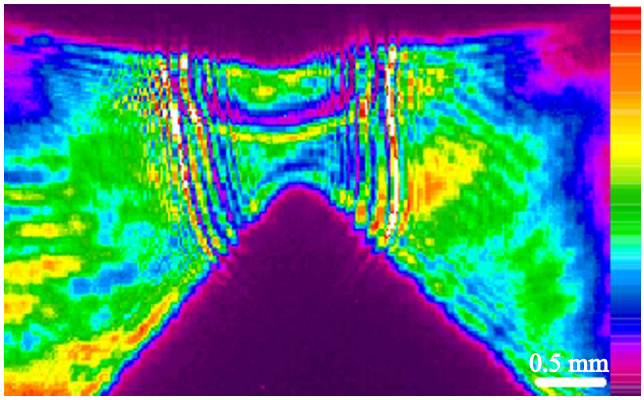

Figure 10. Image of the interelectrode gap cathode–anode. The image was obtained using the optical scheme of shadow probing with parallel beam.

acceleration of the SW front, formed by the current channel of the main discharge, occurs in the time interval $0.4-0.6\,\mu$s after the start? And why, despite the passage through the maximum of the SW velocity, does a monotonous increase in the width of the relaxation zone occur at its front? As an answer, we can present the following assumption based on the analysis of the data given in the publications. Initially, during discharge in gas with characteristic times of the nanosecond range, energy is transferred from the current circuit to the excitation energy of gas molecules. Then, with characteristic times of about $1\,\mu$s, as the excited states of the molecules relax [38,39] their energy is converted into thermal energy or into the translational temperature of gas molecules. Which already leads to a rapid broadening of the current flow area [40–42]. Moreover, the time of vibrational relaxation in oxygen at the same temperature is less than in nitrogen, since the natural frequency in nitrogen is one and a half times greater than in oxygen, which makes it difficult to excite vibrations in nitrogen. Therefore, vibrational relaxation in air has two periods: first, oxygen comes into equilibrium, and then nitrogen. The presence of water vapor, whose molecules actively excite vibrations, can reduce the relaxation time [4]. The dependence of the relaxation time of the energy of molecule vibrations on the degree of compression and temperature is well described by the experimentally verified formula [43]:

$$\tau_{rv} \approx \frac{A}{(\rho/\rho_0)} \exp\left(\frac{B}{\sqrt[3]{T}}\right),$$

where τ_{rv} is relaxation time, ρ/ρ_0 is degree of matter compression behind SW front, T is temperature, A and B are constants, as well as the results of measurements of the vibrational relaxation time in oxygen and nitrogen in shock tube and the parameters of the medium behind the SW front in air under normal conditions, given there, we made some estimates. In the section $0.4-0.6\,\mu$s after the start, when the SW velocity reaches its maximum value, the relaxation times were: for oxygen $\sim 0.2-0.4\,\mu$s and for nitrogen $\sim 2-3\,\mu$s. The effective width of the relaxation zone can be estimated from the relation [4]:

$$\Delta x \approx \frac{7}{9}\frac{D}{(\rho/\rho_0)}\tau_{rv},$$

where Δx is the width of the relaxation zone, D is SW velocity. The estimates gave the following results: $\sim 0.04-0.1$ mm for oxygen and $0.8-1.5$ mm for nitrogen. Comparison with the measured width of the relaxation zone, observed by the method of shadowgraphy in parallel beams, shows that the transition layer is probably nothing but the relaxation zone of oscillations in oxygen. The relaxation zone in nitrogen apparently covers the entire region behind the SW front, which is noticeable from the increased level of probing radiation scattering inside this region in the images obtained using the optical scheme with collimation. Probably, gas with a sufficiently high energy density of molecule vibrations has an increased ability to scatter the optical radiation.

Additionally, attention is drawn to a circumstance that becomes noticeable when the shadow method of image formation is used. The spatial structure of a flat and spherical SW is relatively simple. In the case of cylindrical wave, its spatial structure is quite more complex, namely, consisting of alternating layers of compression and rarefaction (Fig. 10). Apparently, this is a clear demonstration of the results obtained by the methods of mathematical physics. As shown in [35], a sonic cylindrical diverging wave differs significantly from the spherical or plane wave in that it can have a leading front but cannot have a trailing front. When the sound perturbation reaches a given point in space, it no longer stops at it, but only damps relatively slowly asymptotically with time. May be the existence of the relaxation zone of oscillations in oxygen is maintained, and perhaps leads to its growth with time at the cylindrical wave stage precisely due to the unstopped propagation of oscillations inside the cylindrical wave. A confirmation is the fact that when the cylindrical wave transforms into the spherical one, the image of the relaxation zone disappears rather quickly.

Let us briefly comment on two objects observed using the optical scheme with collimation of the probing radiation. One of them is shadowing zone, which is probably located in front of the shock wave front, and the second one is a transition layer, completely opaque to probing radiation, the thickness of which is greatest at the cathode and gradually decreases as it approaches the anode up to full disappearance of the layer. The first object that appears, according to our observations, at the stage of SW acceleration can be associated with the development of the Rayleigh-Taylor instability on the contact surface of the SW and the background gas. A similar phenomenon was predicted theoretically and observed experimentally for laser plasma. The instability development leads first to the growth of small perturbations and then passes into the turbulence stage [44]. As for the second object, it was previously shown by mathematical modeling methods that a stationary flow in the relaxation zone can be unstable with respect to turbulence [4,45]. Therefore, we can suppose that the matter behind the SW, DJ in our case, experiences strong turbulence, which is especially noticeable near the cathode surface, along which the SW moves. The formation of a turbulent layer that cools matter behind the wave front can affect the dynamics of the current channel, which plays the role of piston in SW formation [46]. Probably, in this way, in addition to the above mechanism of excitation of molecule vibrations some „deceleration“ of the process of broadening of the current channel at the initial stage of the discharge can occur. The phenomenon of matter turbulization, i.e. formation of vortex motions in it and accompanying density heterogeneities in the discharge channel after the SW passage, makes additional contribution to the scattering of probing radiation [46], and is therefore especially noticeable in the optical scheme with collimation of probing radiation.

Finally, let us try to comment on the object, which is supposedly a Mach wave. It, as was already noted, is not observed when using the optical scheme with collimation of the probing laser radiation transmitted through the object under study. Consequently, it scatters the probing radiation, but quite weakly. At the same time, when using the optical scheme of shadow probing with parallel beam, it is observed quite distinctly. Based on the above circumstances, we can conclude that this is SW with a high level of excitation of molecular vibrations, but a low level of turbulence in the relaxation zone.

In conclusion, let us perform some estimates of the density of the plasma registered in the discharge. For radiation with wavelength $\lambda \approx 1\,\mu$m the critical electron concentration in plasma is $N_e^{crit} \approx 10^{21}\,\mathrm{cm}^{-3}$. The molecules concentration in air at atmospheric pressure and room temperature is $N_e^{\circ} = 2.4 \cdot 10^{19}\,\mathrm{cm}^{-3}$. In the optical scheme without probing radiation collimation the maximum angle through which the probing beam can deviate without leaving the aperture is $\theta_{\max} \approx 12^{\circ}$. The corresponding electrons concentration is $N_e \approx N_e^{crit} \cdot \sin\theta_{\max} \approx 2 \cdot 10^{20}\,\mathrm{cm}^{-3}$ [5]. According to the data given in [16], on average the relative compaction in SW caused by the discharge in the cathode–anode gap can be 4–6, i.e. $N_e^{SW} \approx (1.0\text{–}1.4) \cdot 10^{20}\,\mathrm{cm}^{-3}$, which is close to the above result $N_e(\theta_{\max} \approx 12^{\circ})$. The recorded width of the density jump in SW in our experiments was $h \approx 10^{-2}$ cm. Accordingly, the electron density gradient is $(N_e - N_e^{\circ})/h \approx 10^{22}\,\mathrm{cm}^{-4}$. In the optical scheme with probing radiation collimation $\theta_{\max} \approx 3^{\circ}$ and $N_e \approx 5 \cdot 10^{19}\,\mathrm{cm}^{-3}$.

Conclusion

The switching process of short (1 mm) gas-filled gap, initiated by auxiliary spark discharge over the surface of dielectric, was studied using the shadow method for visualizing the spatial structure of the matter in the interelectrode gap. The duration of the probing pulse of laser radiation is 2.5 ns; wavelength is $1.06\,\mu$m. Two optical schemes for recording optical images were used, i.e. shadow probing by a parallel beam of rays and the formation of a shadow image by collimating the narrow beam of probing radiation after transmitting through the region of space under study.

In a series of experiments using scheme with collimation directly behind the SW front, the state of matter was observed in which it turns out to be completely optically opaque or strongly scattering the probing radiation. When using the shadow probing method, these areas turn out to be transparent. This circumstance can be explained by the fact that the matter experiences strong turbulence behind the SW front, i.e. in it the formation of vortex motions and accompanying density heterogeneities occur after the shock wave transmission. The formation of the turbulent layer that cools matter behind the wave front can affect the dynamics of the current channel.

The spatial structure of the cylindrical SW observed using the shadow probing method is noticeably more complicated than the spatial structure of the flat and spherical SWs.

The registered dependences of the displacement of the observed SWs on the time elapsed since the start of current flow in the discharge differ from similar dependences given in the publications. At the initial stage, the registered dependences are non-linear. A sudden acceleration of the movement of shock wave fronts is observed in the time interval $0.4\text{–}0.6\,\mu$s after the start, despite the fact that the main part of the energy introduced in the discharge was already released by this time. Possible explanation is preliminary accumulation of input energy in the form of excitation energy of gas molecules.

An object was also found moving along the axis of the main discharge inside the region, already affected by the shock compression process. The object initially has a spherical geometry and is formed on the cathode surface, and then propagates along the main discharge axis towards the anode, acquiring an almost flat shape. The object was identified as SW propagating from the area of the cathode spot of the main discharge.

Conflict of interest

The authors declare that they have no conflict of interest.

References

[1] I.A. Doroshchenko, I.A. Znamenskaya, A.Yu. Kuznetsov, I.V. Mursenkova, N.N. Sysoev. ZhTF, **88** (5), 684 (2018). (in Russian) DOI: 10.21883/TP.2022.10.54358.106-22
[I.A. Doroshchenko, I.A. Znamenskaya, A.Yu. Kuznetsov, I.V. Mursenkova, N.N. Sysoev. Tech. Phys., **63** (5), 662 (2018). DOI: 10.1134/S1063784218050067]

[2] E.M. Barkhudarov, N.K. Berezhetskaya, T.S. Zhuravskaya, V.A. Kol'ev, I.A. Kossy, I.A. Levin, V.V. Markov, N.A. Popov, M.I. Taktakishvili, N.M. Tarasova, N.M. Temchin. TVT, **48** (5), 653 (2010) (in Russian).

[3] S.G. Davydov, A.N. Dolgov, A.V. Korneev, R.Kh. Yakubov. Prikladnaya fizika, **4**, 39 (2019) (in Russian).

[4] Ya.B. Zel'dovich, Yu.P. Raizer, *Fizika udarnykh voln i vysokotemperaturnykh gidrodinamicheskikh yavlenii* (Nauka, M., 1966) (in Russian)

[5] E.D. Vovchenko, A.P. Kuznetsov, A.S. Savelov. *Lazernye metody diagnostiki plasmy: ucheb. posobie* (MIFI, M., 2008) (in Russian)

[6] A.V. Korelsky. *Lasernaya diagnostika plasmy v sil'notochnykh impulsnykh razryadakh* (Cand. diss., MFTI, M., 2005) (in Russian)

[7] V.I. Krauz, M.A. Karakin, V.V. Myalton, V.P. Vinogradov, O.N. Krokhin, V.Ya. Nikulin, A.V. Oginov, A.E. Gurey, A.A. Tikhomirov. Problems of Atomic Science and Technology. Series: Plasma Physics, **1** (10), 212 (2005).

[8] Yu.G. Kalinin, A.V. Korelsky, E.V. Shashkov. Kvant. elektron., **34** (5), 399 (2004) (in Russian).

[9] E.V. Parkevich, S.I. Tkachenko, A.V. Agafonov, A.R. Mingaleev, V.M. Romanova, T.A. Shelkovenko, S.A. Pikuz. ZhETF, **151** (4), 627 (2017) (in Russian).
DOI: 10.7868/S0044451017040010

[10] Liu Tian-Hang, Hao Zuo-Qiang, Gao Xun, Liu Ze-Hao, Lin Jing-Quan. Chin. Phys. B, **23** (8), 7 (2014). DOI: 10.1088/1674-1056/23/8/085203
[11] V.P. Zimakov, N.G. Soloviev, A.N. Shemyakin, A.O. Shilov, M.Yu. Yakimov. Fizikokhimicheskaya kinetika v gazovoj dinamike, **16**(4), 13 (2015). (in Russian)
[12] V.V. Osipov, V.V. Platonov, V.V. Lisenkov. Kvant. elektron., **39** (6), 541 (2009) (in Russian).
[13] T. Perhavec, J. Diaci. Strojniški Vestnik — J. Mechan. Engineer., **56** (7–8), 477 (2010).
[14] G.V. Najdis. TVT, **29** (1), 15 (1991) (in Russian).
[15] I.S. Marshak. UFN, **71** (2), 229 (1962) (in Russian).
[16] A.F. Aleksandrov, A.A. Rukhadze. UFN, **112** (2), 193 (1974) (in Russian).
[17] Ch. Niemann. *Plasma Diagnostics of Discharge Channels for Neutralized Ion-Beam Transport* (Dissertassion zur Erlangung des Grades eines Doctors der Naturwissenschaften. Technicshen Universitä t Darmstadt, 2002)
[18] Kh.G. Akhmedova. Udarnye volny v slaboionizirovannoy plazme (Diss. DGU, Makhachkala, 2009) (in Russian)
[19] S.G. Kalmykov, I.V. Miroshnikov, M.V. Petrenko, M.E. Sasin. Pis'ma v ZhTF, **37** (6), 63 (2011) (in Russian).
[20] K.I. Almazova, A.N. Belonogov, V.V. Borovkov, V.S. Kurbanismailov, P.Kh. Omarova, G.B. Ragimkhanov, D.V. Tereshonok, A.A. Trenkin, Z.R. Khalikova. Fizika plazmy, **47** (1), 75 (2021) (in Russian). DOI: 10.31857/S0367292121010029
[21] V.A. Ivanov, M.E. Konyzhev, A.M. Zimin, V.I. Troinov, T.I. Kamolova, A.A. Letunov. UPF, **2** (1), 31 (2014). (in Russian)
[22] V.G. Borodin, V.M. Komarov, S.V. Krasov, V.A. Malinov, V.M. Migel, N.V. Nikitin, V.N. Chernov, A.V. Charukhchev. Optika atmosfery i okeana, **13** (5), 482 (2000) (in Russian).
[23] O.B. Ananyin, Yu.A. Bykovskii, Yu.V. Eremin, E.L. Stupitskii, I.K. Novikov, S.P. Frolov. Kvant. elektron., **18** (7), 869 (1991) (in Russian).
[24] E.L. Stupitsky, V.A. Andrushchenko. Komp'yuternye issledovaniya i modelirovanie, **12** (3), 505 (2020). (in Russian)
[25] G.A. Mesyats. *Ektony v vakuumnom razryade: proboy iskra, duga* (Nauka, M., 2000) (in Russian).
[26] O.A. Kozhenkova, A.A. Motorin, E.L. Stupitskii. Geomagnetizm i aeronomiya, **53** (5), 620 (2013). (in Russian)
[27] N.A. Ashurbekov, K.O. Iminov. Tech. Phys., **60** (10), 1456 (2015).
[28] S.Z. Sakhapov. *Parametry plazmy sfericheski stratifitsirovannogo gazovogo razryada* (Diss., Institut teplofiziki SO RAN, Novosibirsk, 2008) (in Russian)
[29] O.A. Sinkevich, D.A. Taraskin. TVT, **33** (1), 7 (1995) (in Russian).
[30] K.N. Mitrofanov. *Eksperimental'noe issledovanie osobennostej plazmoobrazovaniya i tokovogo szhatiya plazmy lajnerov razlichnykh konstruktsij* (Diss. AO „Gosudarstvennyj nauchnyj tsentr Rossijskoj Federatsii Tritskij i9nstitut innovatsionnykh i termoyadernykh issledovanij", M., 2019) (in Russian)
[31] S.G. Davydov, A.N. Dolgov, A.A. Kozlov, R.Kh. Yakubov. Tekhnologii EMS, **78**, (3), 20 (2021). (in Russian).
[32] L.P. Babich. UFN, **175** (10), 1069 (2005) (in Russian).
[33] O.A. Omarov, A.A. Rukhadze. Prikladnaya fizika, **4**, 24 (2010) (in Russian).
[34] S.G. Davydov, A.N. Dolgov, A.A. Kozlov, R.Kh. Yakubov. Prikladnaya fizika, **4**, 19 (2021) (in Russian). DOI: 10.51368/1996-0948-2021-4-19-24
[35] L.D. Landau, E.M. Lifshitz, *Teoreticheskaya fizika: uchebnoe posobie: dlya vuzov. V 10 t. T. VI, Gidrodynamika*. 5 izd. sterotip. (Fizmatlit, M., 2003) (in Russian).
[36] M. Corsi, G. Cristoforetti, M. Hidalgo, D. Iriarte, S. Legnaioli,V. Palleschi, A. Salvetti, E. Tognoni. Appl. Spectrosc., **59**, 853 (2005).
[37] N.N. Gladyshev. *Gidrogazodinamika: konspekt lektsij* (GOUVP SPbGTURP, SPb., 2012) (in Russian)
[38] K.G. Owen. *Measurements of Vibrational Relaxation and Dissociation of Oxygen with Laser Absorption Spectroscopy with Applications for Energy Transfer in Nonequilibrium Air* (Stanford University, 2014)
[39] A.I. Bechina, E.V. Kustova. Vestnik Sankt-Peterburgskogo universiteta. Matematika. Mekhanika. Astronomiya, №6 (1), 118 (2019) (in Russian).
[40] I. Znamenskaya, E. Koroteeva, I. Doroshchenko. Phys. Fluids, **32** (9), 1 (2020). DOI: 10.1063/5.0019016.
[41] D.A. Xu, D.A. Lacoste, C.O. Laux. IEEE Transactions on Plasma Science PSI, **42** (10), 2350 (2014). DOI: 10.1109/TPS.2014.2311328
[42] I.A. Znamenskaya, I.A. Doroshenko, D.S. Naumov, T.A. Kulizade. Nauchnaya vizualizatsiya, **10** (9), 3 (77) (in Russian).
[43] G.K. Vasil'ev, E.F. Makarov, V.G. Papin, V.L. Tal'roze. Sov. Phys. JETP, **37** (6), 1031 (1973).
[44] O.B. Ananyin, Yu.A. Bykovskii, Yu.V. Eremin, E.L. Stupitskii, I.K. Novikov, S.P. Frolov. Kvant. elektron., **8** (7), 869 (1991) (in Russian).
[45] N.M. Kuznetsov. UFN, **159** (3), 493 (1989) (in Russian).
[46] M.N. Schneider. TBT, **32** (1), 57 (1994).